# An NMR-Derived Model for the Solution Structure of Oxidized Putidaredoxin, a 2-Fe, 2-S Ferredoxin from *Pseudomonas*†,‡

Thomas C. Pochapsky,*,§ Xiao Mei Ye,§,‖ Gayathri Ratnaswamy,§ and Teresa A. Lyons⊥

*Departments of Chemistry and Biology, Brandeis University, Waltham, Massachusetts 02254-9110*

*Received December 16, 1993; Revised Manuscript Received March 23, 1994*®

ABSTRACT: A model for the solution structure of oxidized putidaredoxin (Pdx), a 106-residue globular protein containing a $Fe_2S_2$ cluster, has been determined using homonuclear NMR methods. Pdx is the first of the class of $Fe_2S_2Cys_4$ ferredoxins which act as electron-transfer partners for P-450 monooxygenases to be structurally characterized, and no crystal structure has been determined for Pdx or for any closely homologous protein. Pdx is the physiological redox partner of cytochrome $P\text{-}450_{cam}$. A total of 878 NOE distance constraints, 66 $\phi$ angular constraints derived from NH–$C_\alpha$H coupling constants, and five paramagnetic broadening constraints were used in simulated annealing structural refinements to obtain a family of structures with pairwise rms deviations of 1.14 Å for backbone atoms and 1.80 Å for all non-hydrogen atoms. Paramagnetic broadening of resonances within a ca. 8-Å radius of the metal cluster prevents the use of NMR-derived constraints in this region of the protein; structural constraints used to model the environment of the metal cluster were obtained from site-directed mutagenesis and model compounds and by comparison with known ferredoxin structures. Pdx retains a similar folding topology to other structurally characterized $Fe_2S_2Cys_4$ ferredoxins but differs from the other ferredoxins in containing a significantly more compact structure in the C-terminal half of the protein.

Electron transfer in living organisms must be tightly regulated in both space and time in order to prevent "short circuits", that is, rapid equilibration across chemical potential gradients. The mechanisms involved in such regulation are not well understood and are the subject of much current debate (McLendon, 1988; Thomson, 1991). Kinetic and mechanistic studies have provided much information on biological electron transfer (Moser et al., 1992; Beratan et al., 1992), but structural data on the proteins involved are critical if an understanding of the mechanism(s) of electron transfer at the molecular level is to be gained.

One of the best-studied electron-transfer systems is the camphor hydroxylase system isolated from *Pseudomonas putida* grown on media containing camphor as the sole carbon source. Three proteins, $P\text{-}450_{cam}$, putidaredoxin reductase (PdR), and putidaredoxin (Pdx)[1] make up this system [for a review, see Murray et al. (1985)]. $P\text{-}450_{cam}$ catalyzes the 5-*exo*-hydroxylation of camphor by molecular oxygen. The FAD-containing PdR catalyzes the two-electron oxidation of NADH to $NAD^+ + H^+$. Pdx is a small (106-residue) ferredoxin containing a single $Fe_2S_2Cys_4$ cluster (Cushman et al., 1967). Pdx accepts a single electron from PdR, which it then transfers to $P\text{-}450_{cam}$. Camphor hydroxylation requires two electrons per turnover, and so two discrete binding events between $P\text{-}450_{cam}$ and Pdx are required per turnover. The reduction potential of Pdx ($E_{obs} = -196$ mV) is such that only the substrate-bound form of $P\text{-}450_{cam}$ ($E_{obs} = -173$ mV) is reduced by Pdx. (The $E_{obs}$ of substrate-free $P\text{-}450_{cam}$ is $-303$ mV.) Pdx also plays an effector role in this reaction, as kinetic evidence suggests that the diprotein complex is the active species for camphor hydroxylation (Lipscomb et al., 1976).

This exquisitely regulated and complex redox pairing provides an ideal case study for the scientist interested in biological electron transfer and molecular recognition. $P\text{-}450_{cam}$ is one of the few P-450s for which a structure has been determined (Poulos et al., 1987; Ravichandran et al., 1993). Regulation of the $P\text{-}450_{cam}$ reduction potential by substrate has been described in detail (Gunsalus & Sligar, 1978; Sligar et al., 1974a). However, the wealth of thermodynamic, kinetic, and mechanistic data available concerning the Pdx/$P\text{-}450_{cam}$ couple has been difficult to interpret owing to the lack of structural information for Pdx (Baldwin et al., 1991; Halliwell, 1991). Despite many efforts, Pdx has resisted crystallization, and in order to facilitate an understanding of the complex interactions between these two proteins, we have undertaken the determination of the solution structure of oxidized Pdx using NMR methods. Recently, we reported extensive sequential $^1H$ resonance assignments and described the secondary structural elements of oxidized Pdx (Pochapsky & Ye, 1991; Ye et al., 1992). We now describe a model for the solution structure of Pdx, as determined by analysis of nuclear Overhauser effects, *J*-coupling information, and other experimental data.

## EXPERIMENTAL PROCEDURES

Samples of oxidized putidaredoxin were obtained, purified, and prepared for NMR spectroscopy as described previously (Pochapsky & Ye, 1991). Spectroscopic methods and as-

† This work was supported by a grant from the National Institutes of Health (GM-44191, T.C.P.). T.C.P. acknowledges support by the NSF Young Investigator Program (CHE-9257036) and the Camille and Henry Dreyfus Teacher–Scholar Program.

‡ PDB files for the set of 10 structures for oxidized Pdx have been deposited with the Brookhaven Protein Data Bank or can be obtained from the author at *pochapsky@binah.cc.brandeis.edu*.

* To whom correspondence should be addressed.

§ Department of Chemistry.

‖ Current address: Sloan-Kettering Cancer Research Inst., NY.

⊥ Department of Biology.

® Abstract published in *Advance ACS Abstracts*, May 1, 1994.

[1] Abbreviations: DQF-COSY, double-quantum-filtered *J*-correlated spectroscopy; fid, free induction decay; FAD, flavin adenine dinucleotide; NADH, nicotinamide adenine dinucleotide; NMR, nuclear magnetic resonance; NOE, nuclear Overhauser effect; NOESY, two-dimensional NOE spectroscopy; PdR, putidaredoxin reductase; Pdx, putidaredoxin; PE-COSY, primitive exclusive *J*-correlated spectroscopy; rmsd, root-mean-square deviation.

0006-2960/94/0433-6424$04.50/0 

signment methodologies used for $^1H$ sequential assignments have also been detailed previously (Ye et al., 1992).

*NMR Experiments.* A series of NOESY experiments using mixing times of 10, 20, 30, 50, 70, and 90 ms were performed on a Bruker AMX-600 spectrometer operating at 600 MHz ($^1H$) on a sample of 3 mM oxidized Pdx (290 K in 90%/10% $H_2O/D_2O$, pH 7.4, 10 mM Tris-$d_6$ buffer). Water suppression was achieved by presaturation, and a standard pulse sequence was used (Kumar et al., 1980). Phase sensitivity in the $t_1$ dimension was obtained using time-proportional phase incrementation (TPPI). Data was processed and analyzed using volume integration and comparison facilities in the FELIX 2.1 software package (Biosym Technologies).

The homonuclear double-quantum experiment was performed using the sequence of Rance et al. with double-quantum mixing times of 5, 10, 20, 30, and 40 ms (Rance et al., 1989). The PE-COSY experiment was performed on solutions of oxidized Pdx in $D_2O$ (Mueller, 1987). Phase sensitivity in the $t_1$ dimension was obtained using the method of States et al. (States et al., 1982). Dispersive diagonal elements in the PE-COSY spectrum were removed by subtracting a two-dimensional spectrum containing only diagonal peaks from the PE-COSY data set. The diagonal spectrum was generated by shifting the first fid by one point for each increment of $t_1$, storing the fids thus generated as a two-dimensional matrix, and processing as for the two-dimensional PE-COSY (Marion & Bax, 1988).

*NOE Constraints.* On the basis of examination of NOESY data sets obtained at different mixing times, NOESY spectra obtained with a 70-ms mixing time were determined to be essentially free of correlations due to spin diffusion, and the volume of NOE cross peaks at this mixing time were taken to be proportional to the inverse sixth power of the distance between the connected protons. NOE intensities were defined as very strong, strong, medium, and weak. Distance constraints were applied as follows. Very strong NOEs were assigned distances of 2.0–2.5 Å, strong NOEs 2.0–3.0 Å, medium NOEs 2.0–4.0 Å, and weak NOEs 2.0–5.0 Å. Pseudoatom constraints as described by Wüthrich were used to adjust distances involving methyl groups (by adding 1 Å), aromatic ring protons (by adding 2.4 Å to constraints involving $C_\delta H$ and $C_\epsilon H$ aromatic protons of tyrosine and phenylalanine), and diastereotopic methylene protons (by adding 1 Å) (Wüthrich et al., 1983).

A total of 878 NOE distance constraints were used in the calculations, including 378 local interresidue constraints (between residues $i$ and $j$ where $|i - j| \leq 3$), 344 nonlocal constraints ($|i - j| > 3$), and 156 intraresidue constraints. This represented virtually all of the NOE constraints that could be unambiguously identified in NOESY spectra and corresponded to an average of 9.8 NOEs for each spectroscopically identified residue (i.e., those unaffected by paramagnetic broadening). Further increases in the number of NOE constraints would require the use of heteronuclear-edited multidimensional NMR methods. A scatter plot of interresidue NOEs used as constraints is shown in Figure 1. Sequential NOEs indicating secondary structure are shown in Figure 2.

*Dihedral Angle Constraints and Stereospecific Assignments.* $\phi$ backbone dihedral angle constraints (C–N–$C_\alpha$–C) used for regions of the protein directly observable by NMR were estimated from the magnitude of $^3J_{HN-C_\alpha H}$ using the Karplus relationship (Pardi et al., 1984). NH–$C_\alpha$H coupling constants were either measured from linear combinations of 2QF-COSY and NOESY data using the difference methods

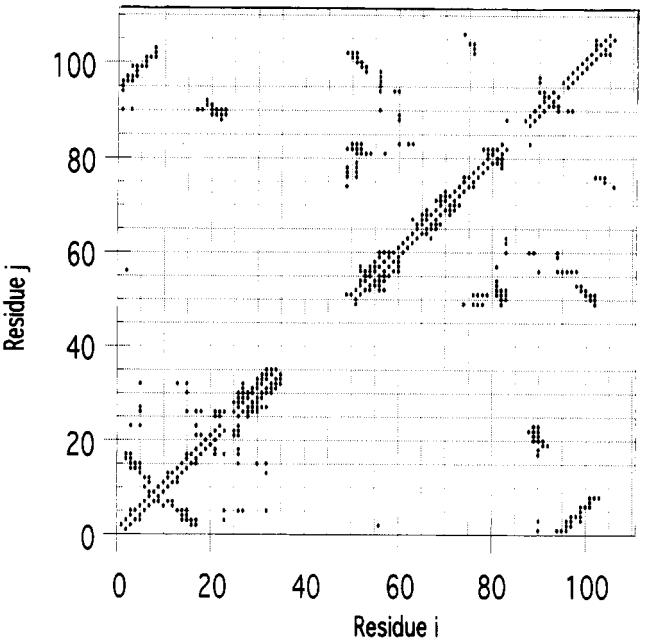


FIGURE 1: Interresidue NOEs identified in oxidized Pdx and used as constraints for structural calculations. For clarity, only one point is generated for each pair of amino acid resides $i$ and $j$ which have been connected by NOEs, even if multiple NOEs have been observed between the pair.

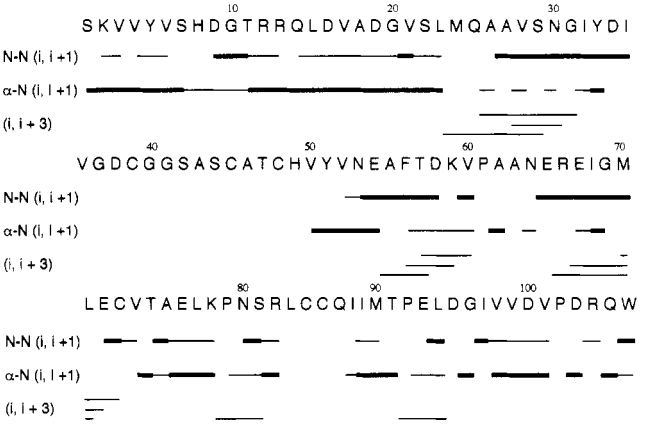


FIGURE 2: Sequential NOEs used to identify secondary structural features in oxidized Pdx and used as constraints in the structural calculations. Heavy lines indicate strong NOEs; thinner lines represent weaker NOEs. N–N ($i$, $i + 1$) refers to NOEs between the NH protons of adjacent residues; $\alpha$–N ($i$, $i + 1$) refers to a NOE between the $C_\alpha$H of residues $i$ to the NH of residue $i + 1$. Connectivities indicated by $i$, $i + 3$ refers to the observation of either $C_\alpha$H–NH or $C_\alpha$H–$C_\beta$H connectivity. The sequence is that of Koga et al. (1989). Sequence numbers are provided at 10-residue intervals.

of Poulsen (Ludvigsen et al., 1991) or, for residues of which the NH–$C_\alpha$H cross peaks are lost due to overlap with the water resonance in 2QF-COSY and NOESY spectra, estimated from the buildup of the NH–$C_\alpha$H correlations in double-quantum spectra as a function of mixing time (Ratnaswamy and Pochapsky, manuscript in preparation). A graph of $^3J_{HN-C_\alpha H}$ versus residue number is shown in Figure 3. In this manner, 66 $\phi$ angle constraints were obtained. Because of the imprecision of measuring coupling constants by these methods, all $\phi$ angle constraints were set so as to allow deviations of up to 40° in either direction without penalty.

Only one $\chi_1$ angular constraint was applied explicitly (for Thr 57); the high degree of overlap encountered in the $C_\alpha$H–$C_\beta$H region of the PE-COSY experiment prevented measurement of both $^3J_{\alpha\beta}$ and $^3J_{\alpha\beta'}$ in most cases, which, along with NOE information, is required to distinguish between possible

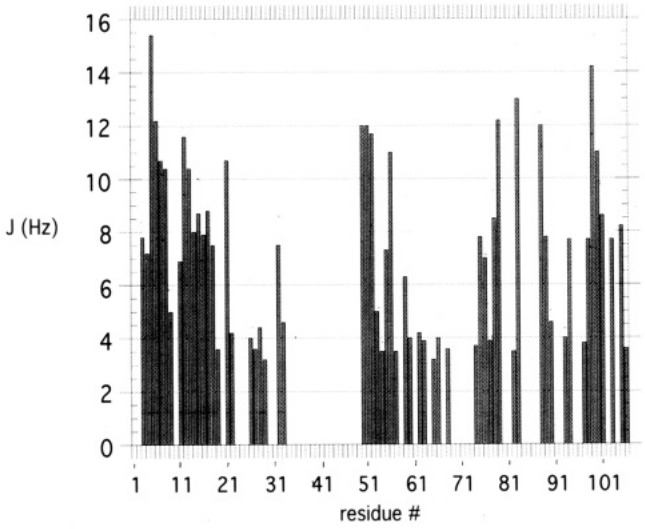


FIGURE 3: Bar graph of $^3J_{NH-C\alpha H}$-coupling constants (Hz) for oxidized Pdx, measured as described in Experimental Procedures.

$\chi_1$ angles for side chains containing diastereotopic $CH_2$ groups (Nagayama & Wuthrich, 1981; Smith et al., 1991). The assignments for only two sets of diastereotopic $CH_2$ groups, those of Asn 64 and Asn 81, could be confirmed by complete characterization of $^3J_{\alpha\beta}$ and $^3J_{\alpha\beta'}$ and the required NOEs (Kraulis et al., 1989). Stereospecific assignments were confirmed for the diastereotopic methyl groups of Val 17 and Val 60 by a combination of NOE and $^3J_{\alpha\beta}$-coupling information (Zuiderweg et al., 1985; Arseniev et al., 1988). Stereospecific assignments in all other cases were made from the best fit of observed NOE patterns for distinguishable resonances of diastereotopic protons or methyl groups with those expected from the multiple structures generated using pseudoatom NOE constraints on the diastereotopic groups (Kline et al., 1990). These assignments are shown in Table 1.

*Modeling of the $Fe_2S_2Cys_4$ Cluster and Environment.* Antiferromagnetic coupling of the two iron atoms renders oxidized Pdx diamagnetic at low temperatures (Poe et al., 1971). However, thermal population of electronic states with $S > 0$ gives rise to unpaired electron-spin density at ambient temperatures (Ratnaswamy & Pochapsky, 1993). This introduces a serious complication into the process of determining a solution structure for Pdx by NMR, as severe line broadening and rapid relaxation are observed for resonances close to the metal center. Resonances remaining unidentified due to broadening include the entire spin systems of residues 36–48 and 84–86 and portions of the spin systems of residues 24, 25, 49, 70, 71, and 87. Attempts to use methodologies developed in other laboratories for sequential identification of hyperfine-shifted and -broadened resonances failed in the present case because of the exceedingly short relaxation times of nuclei near the metal cluster (Dugad et al., 1990; Ratnaswamy & Pochapsky, 1993).

Therefore, in order to generate a structural model for Pdx from the available NOE and coupling information, a model for the metal cluster and its environment was needed. The model must account for a number of observations. First, mutagenesis experiments indicate that four of the six cysteines in Pdx are required for correct folding and incorporation of the metal cluster, Cys 39, Cys 45, Cys 48, and Cys 86, while Cys 73 and Cys 85 are not (Gerber et al., 1990). Our previous assignment of the $^1H$ resonances of Cys 73 confirmed that this residue is further than 8 Å from the metal center (Ye et al., 1992). More recently, $^1H$ NMR characterization of Pdx

Table 1: Best-Fit Stereospecific $^1H$ Resonance Assignments for Oxidized Pdx, pH 7.4, 17 °C[a]

| residue | assignment |
|---|---|
| Ser 1 | $C_{\beta 1}H$ 3.57; $C_{\beta 2}H$ 3.40 |
| Lys 2 | $C_{\beta 1}H_2$ 1.29; $C_{\beta 2}H$ 1.55 |
| Val 3 | $C_{\gamma 1}H_3$ 0.04; $C_{\gamma 2}H_3$ 0.45 |
| Val 4 | $C_{\gamma 1}H_3$ 0.53; $C_{\gamma 2}H_3$ 0.49 |
| Tyr 5 | $C_{\beta 1}H$ 2.23; $C_{\beta 2}H$ 2.72 |
| Val 6 | $C_{\gamma 1}H_3$ 0.72; $C_{\gamma 2}H_3$ 0.56 |
| Arg 13 | $N_{\eta 1}H_2$ 6.23; $N_{\eta 2}H_2$, 7.20 |
| Leu 15 | $C_{\beta 1}H$ 1.31; $C_{\beta 2}H$ 1.23; $C_{\delta 1}H_3$ 0.60; $C_{\delta 2}H_3$ 0.52 |
| *Val 17 | $C_{\gamma 1}H_3$ 0.66; $C_{\gamma 2}H_3$ 0.58 |
| Gly 20 | $C_{\alpha 1}H$ 3.23; $C_{\alpha 2}H$ 4.08 |
| Val 21 | $C_{\gamma 1}H_3$ 0.89; $C_{\gamma 2}H_3$ 0.62 |
| Leu 23 | $C_{\delta 1}H_3$ 0.57; $C_{\delta 2}H_3$ 0.52 |
| Val 28 | $C_{\gamma 1}H_3$ 0.75; $C_{\gamma 2}H_3$ 0.68 |
| *Asn 30 | $C_{\beta 1}H$ 2.60; $C_{\beta 2}H$ 2.28 |
| Gly 31 | $C_{\alpha 1}H$ 3.55; $C_{\alpha 2}H$ 3.33 |
| Val 50 | $C_{\gamma 1}H_3$ 0.71; $C_{\gamma 2}H_3$ 0.38 |
| Tyr 51 | $C_{\beta 1}H$ 2.69; $C_{\beta 2}H$ 2.62 |
| Val 52 | $C_{\gamma 1}H_3$ 0.81; $C_{\gamma 2}H_3$ 0.66 |
| Asn 53 | $C_{\beta 1}H$ 2.57; $C_{\beta 2}H$ 2.79; $N_{\delta}H_{21}$ 7.08; $N_{\delta}H_{22}$ 8.04 |
| Phe 56 | $C_{\beta 1}H$ 2.57; $C_{\beta 2}H$ 2.98 |
| *Val 60 | $C_{\gamma 1}H_3$ 0.87; $C_{\gamma 2}H_3$ 0.80 |
| Pro 61 | $C_{\beta 1}H$ 2.18; $C_{\beta 2}H$ 1.71; $C_{\gamma 1}H$ 1.84; $C_{\gamma 2}H$ 1.97; $C_{\delta 1}H$ 3.44; $C_{\delta 2}H$ 3.84 |
| *Asn 64 | NH $C_{\beta 1}H$ 3.15; $C_{\beta 2}H$ 2.75 |
| Val 74 | $C_{\gamma 1}H_3$ 0.37; $C_{\gamma 2}H_3$ 0.68 |
| Glu 77 | $C_{\beta 1}H$ 1.81; $C_{\beta 2}H$ 1.58 |
| Leu 78 | $C_{\delta 1}H_3$ 0.82; $C_{\delta 2}H_3$ 0.67 |
| Pro 80 | $C_{\beta 1}H$ 2.28; $C_{\beta 2}H$ 1.76; $C_{\gamma 1}H$ 1.93; $C_{\gamma 2}H$ 2.14; $C_{\delta 1}H$ 3.52; $C_{\delta 2}H$ 3.70 |
| Asn 81 | $N_{\delta}H_{21}$ 7.45; $N_{\delta}H_{22}$ 6.54 |
| Ser 82 | $C_{\beta 1}H$ 3.98; $C_{\beta 2}H$ 3.90 |
| Arg 83 | $N_{\eta 21}H$ 8.37; $N_{\eta 22}H$ 5.50 |
| Leu 94 | $C_{\beta 1}H$ 1.39; $C_{\beta 2}H$ 1.88; $C_{\delta 1}H_3$ 0.60; $C_{\delta 2}H_3$ 0.78 |
| Asp 95 | $C_{\beta 1}H$ 2.74; $C_{\beta 2}H$ 2.48 |
| Gly 96 | $C_{\alpha 1}H$ 4.02; $C_{\alpha 2}H$ 2.82 |
| Val 98 | $C_{\gamma 1}H_3$ 0.61; $C_{\gamma 2}H_3$ 0.75 |
| Val 99 | $C_{\gamma 1}H_3$ 0.36; $C_{\gamma 2}H_3$ 0.30 |
| Val 101 | $C_{\gamma 1}H_3$ 0.72; $C_{\gamma 2}H_3$ 0.58 |
| Pro 102 | $C_{\beta 1}H$ 2.02; $C_{\beta 2}H$ 1.72 |

[a] Assignments are those most consistent with observed NOE patterns, based on examination of multiple structures generated using pseudoatom constraints on the diastereotopic groups. Assignments marked with an asterisk are confirmed by combined coupling constant and NOE information (Kraulis et al., 1989).

in which Cys 85 had been mutated to a serine shows its structure to be indistinguishable from that of the wild-type protein, thereby confirming the previous assignments of the four ligating cysteines (A. Davidson, unpublished results).

Resonance Raman comparison of plant-type ferredoxins and Pdx suggest only minor structural differences between their metal clusters (Fu et al., 1992). A high degree of structural homology exists between some regions of Pdx and the *Anabaena* ferredoxin [particularly the large $\beta$-sheet and $\alpha$-helix observed on the right-hand side of both molecules as viewed in Figures 4 and 5 (Rypniewski et al., 1991)]. Patterns of paramagnetic broadening in Pdx (including the complete spin systems of residues 36–48 and 84–86 and portions of residues 22, 24, 49, 50, 67, 70, 71, 83, 87, and 105) indicate that the position of the cluster is roughly analogous to those of the metal clusters of other $Fe_2S_2Cys_4$ ferredoxins from *Spirulina platensis* and *Anabaena* 7120 (Tsukihara et al., 1981; Rypniewski et al., 1991; Pochapsky et al., 1994). In particular, one residue for which side-chain resonances are lost due to broadening is Met 24 in Pdx (indicated in Figure 4). Met 24 is structurally homologous with Leu 27 in *Anabaena* 7120 ferredoxin (indicated in Figure 5), the side chain of which is broadened by the metal cluster in NMR spectra of that protein (Oh & Markley, 1990). Sequence similarity is low between Pdx and the cyanobacterial ferre-

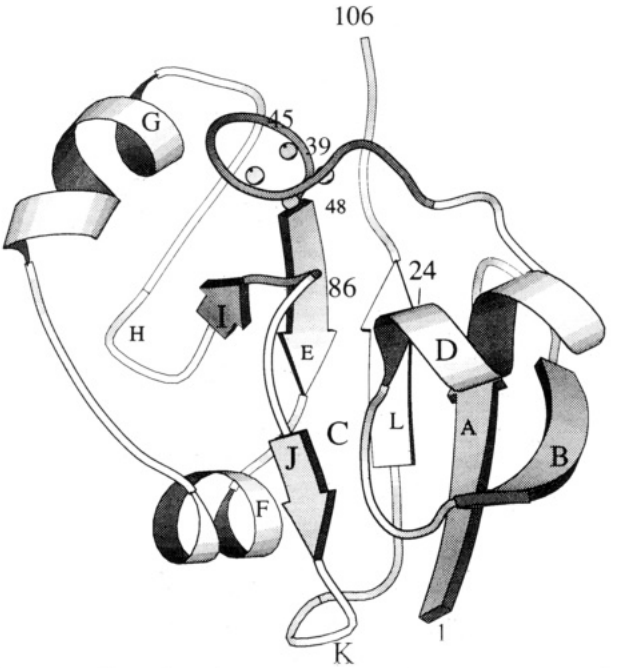


FIGURE 4: Secondary structural domains in oxidized Pdx. The proximal side of the protein (as it is referred to in the text) faces the reader, while the distal side faces away. Lettering corresponds to letter names for secondary structural units described in the text, and numbers refer to sequence positions of the N- and C-terminal residues (Ser 1 and Trp 106) and the cysteinyl ligands for the metal cluster (Cys 39, Cys 45, Cys 48, and Cys 86). The backbone regions containing these residues (Val 36–His 49 inclusive and Leu 84–Cys 86 inclusive) are shaded darker to indicate the extent of backbone structure for which no $^1$H resonance assignments are available and hence no direct structural information exists. The position of Met 24 in helix D, the side-chain resonances of which cannot be observed due to paramagnetic broadening, has been noted for comparison with the *Anabaena* 7120 ferredoxin structure (Figure 5). For clarity, the short $\beta$-strand C has not been indicated by a ribbon. Residues corresponding to domains are as follows: A (Ser 1–Val 6), B (Arg 12–Val 17), C (Val 21 and Ser 22), D (Leu 23–Gly 31), E (Val 50–Asn 53), F (Ala 57–Pro 61), G (Glu 65–Cys 73), H (Lys 79–Ser 82), I (Ser 82–Arg 83), J (Gln 87–Met 90), K (Thr 91–Leu 94), and L (Ile 97–Val 101).


FIGURE 5: Ribbon structure of *Anabaena* 7120 ferredoxin (Rypniewski et al., 1991). Note significant structural homology between Pdx (Figure 4) and the *Anabaena* ferredoxin in the right-hand sides of both molecules as presented, including the four strands of $\beta$-sheet and the short $\alpha$-helical region. Residues Leu 27 (*Anabaena*) and Met 24 (noted in Figure 4), both marked at the position of their $C_\beta$ atoms by their residue numbers, show paramagnetic broadening, indicating a similar placement of the metal cluster in both proteins (Ye et al., 1992; Oh & Markley, 1990).

Table 2: Structural Constraints Used To Model the $Fe_2S_2$ Cluster and Ligating Cysteines in Oxidized Pdx[a]

| Bond Lengths (Å) and Angles (deg) within the Cluster | | | |
|---|---|---|---|
| Fe–S | 2.20 | Fe–S–$C_\beta$ | 109.5 |
| Fe–Fe | 2.72 | S–Fe–S | 105.0 |
| | | Fe–S–Fe | 75.0 |

| Distance Constraints (Å) on Ligating Cysteines | |
|---|---|
| $C_\alpha$ (Cys 39)–$C_\alpha$ (Cys 45) | 6.5 (±0.7) |
| $C_\alpha$ (Cys 45)–$C_\alpha$ (Cys 48) | 7.5 (±0.7) |
| $C_\alpha$ (Cys 48)–$C_\alpha$ (Cys 86) | 6.1 (±0.7) |
| $C_\alpha$ (Cys 39)–$C_\alpha$ (Cys 86) | 8.6 (±0.7) |
| $C_\alpha$ (Cys 39)–$C_\alpha$ (Cys 48) | 9.0 (±0.7) |
| $C_\alpha$ (Cys 45)–$C_\alpha$ (Cys 86) | 6.5 (±0.7) |

| Dihedral Angle Constraints (deg) on Ligating Cysteines | |
|---|---|
| N–$C_\alpha$–$C_\beta$–$S_\gamma$ (Cys 39) | 90 (±40) |
| N–$C_\alpha$–$C_\beta$–$S_\gamma$ (Cys 45) | 90 (±40) |
| N–$C_\alpha$–$C_\beta$–$S_\gamma$ (Cys 48) | 110 (±40) |
| N–$C_\alpha$–$C_\beta$–$S_\gamma$ (Cys 86) | 80 (±40) |
| $C_\alpha$–$C_\beta$–$S_\gamma$–$Fe_1$ (Cys 39) | –65 (±40) |
| $C_\alpha$–$C_\beta$–$S_\gamma$–$Fe_1$ (Cys 45) | –65 (±40) |
| $C_\alpha$–$C_\beta$–$S_\gamma$–$Fe_2$ (Cys 48) | –140 (±40) |
| $C_\alpha$–$C_\beta$–$S_\gamma$–$Fe_2$ (Cys 86) | –120 (±40) |

[a] Bond lengths and angles within the cluster were those found crystallographically for model compounds (Mayerle et al., 1975). Constraints on the ligating cysteines are based on corresponding angles and distances in the *Anabaena* ferredoxin structure (Rypniewski et al., 1991). Bond distances and angles within the metal cluster were subject to the same violation penalties as other covalent bonds. Interresidue distances were treated as NOE constraints, and dihedral angle constraints were used in the same manner as those derived from coupling constants (see text).

doxins (~10%). However, the folding topologies of all three proteins are nearly identical, and what little sequence similarity exists is greatest in the vicinity of the metal cluster binding sites (Pochapsky & Ye, 1991). All of this evidence suggests a similar placement for the metal center in both proteins relative to these structural features. For these reasons, ligation stereochemistry at the iron atoms and cluster geometry for the present model were chosen to match those in known ferredoxin structures (Cys 39 and Cys 45 ligating one iron atom, Cys 48 and 86 ligating the other).

In the *Anabaena* structure, the $\alpha$-carbon atoms of the four cysteinyl ligands describe a rough rectangle. Using the edges and diagonals of the rectangle as constraints on the $\alpha$-carbon atoms of the cysteinyl ligands in Pdx proved to be the most efficient way of maintaining cluster geometry similar to that found in the *Anabaena* protein. $C_\alpha$–$C_\beta$–S–Fe dihedral angles in the cluster were also constrained loosely (±40°) to match the analogous angles in *Anabaena*. Fe–S bond lengths and angles used were those observed in model compounds (Mayerle et al., 1975). Constraints on the metal cluster region are summarized in Table 2.

*Compactness Requirement for the Metal-Binding Site.* One criterion that was applied to judging the validity of any constraint set used to model the metal cluster and vicinity is that of maintaining structural compactness. Electron self-exchange in half-reduced samples of Pdx is quite slow (≤66 $M^{-1}$ $s^{-1}$ at 290 K, Pochapsky et al., accompanying paper), an observation that is incompatible with any structural model that significantly exposes the metal cluster to solvent. Outer sphere electron transfers not involving structural reorganization are very fast if the metal coordination spheres come into contact, with unimolecular rate constants of $10^{10}$ $s^{-1}$ in the

Table 3: Backbone Dihedral Angle ($\phi$, $\psi$) Constraints (deg) on Residues Asp 38–Cys 48 and Leu 84–Gln 87 Used in Calculating Pdx Structural Models which Are Based on Analogy to the Metal Cluster-Binding Loop of *Anabaena* Ferredoxin (Rypniewski et al., 1990)[a]

| | | | | | | | | | |
|---|---|---|---|---|---|---|---|---|---|
| $\phi$ | −130 | −70 | | | | | −120 | −140 | −120 |
| $\psi$ | −80 | −30 | | | | | 20 | −170 | 10 |
| **Pdx** | **D** | **C** | **G** | **G** | **S** | **A** | **S** | **C** | **A** |
| | **38** | **39** | **40** | **41** | **42** | **43** | **44** | **45** | **46** |
| **Fdx** | **S** | **C** | | **R** | **A** | **G** | **A** | **C** | **S** |
| | **40** | **41** | | **42** | **43** | **44** | **45** | **46** | **47** |
| $\phi$ | −133 | −74 | | | | | −120 | −144 | −120 |
| $\psi$ | −76 | −29 | | | | | 20 | −170 | 3 |
| $\phi$ | −50 | −70 | | −100 | −60 | −70 | −130 | | |
| $\psi$ | −50 | 0 | | 100 | −30 | −10 | 20 | | |
| **Pdx** | **T** | **C** | ••••• | **L** | **C** | **C** | **Q** | | |
| | **47** | **48** | | **84** | **85** | **86** | **87** | | |
| **Fdx** | **T** | **C** | | **L** | **T** | **C** | **V** | | |
| | **48** | **49** | ••••• | **77** | **78** | **79** | **80** | | |
| $\phi$ | −53 | −74 | | −96 | −58 | −71 | −131 | | |
| $\psi$ | −49 | −4 | | 103 | −25 | −14 | 20 | | |

[a] The two lines above the Pdx residues indicate angular constraints on Pdx, while the two lines below Fdx (ferredoxin) are observed angles in the *Anabaena* ferredoxin structure (rounded off to the nearest degree). All Pdx dihedral angle constraints include an allowed deviation of ±40° without energetic penalty.

absence of thermodynamic barriers (Williams, 1990). Analysis of electron self-exchange rates in heme proteins suggests that a large fraction of electron transfers occur through exposed heme edges (Dixon et al., 1989), and most heme proteins show electron self-exchange rates between $10^2$ and $10^7$ $M^{-1}$ $s^{-1}$ (Dixon & Hong, 1990). Thus, the slow electron self-exchange observed in Pdx suggests that surface exposure of the metal center is very small.

Ligation stereochemistry at the metal cluster differing from that of *Anabaena* or *Spirulina* ferredoxins resulted for all calculations in noncompact conformations of the polypeptide chain between residues 36 and 49 for Pdx. Furthermore, in order to maintain compactness, the polypeptide chain in the metal cluster-binding site must maintain a conformation similar to that observed in the binding loop of the *Anabaena* 7120 and *Spirulina* ferredoxins. The most straightforward way of accomplishing this is to map the $\phi$–$\psi$ angles of non-glycinyl residues in the *Anabaena* metal-binding site into loose constraints on homologous residues in the Pdx metal-binding site. These constraints are shown in Table 3. For non-glycinyl residues without homologous residues in *Anabaena* (Ser 42, Ala 43, His 49), constraints were set so as to permit negative $\phi$ angles normally found in either extended or compact conformations (−100 ± 40°) and $\psi$ angles were not constrained. Val 36 proved unusual in that this residue required constraint to an extended conformation ($\phi$ = −130 ± 40°) in order to maintain the compactness ($\psi$ was not constrained for Val 36). These constraints are summarized in Table 3.

We conclude, based on extensive dynamics simulations using a variety of constraint sets involving the metal cluster, that the one described here represents the minimum that will generate a structure for Pdx consistent with all experimental data. The geometries and coordinates for the metal cluster and its environment obtained with this set satisfied experimental constraints without inducing localized stress in the observable portions of the structure as well as positioning the metal center so as to rationalize observed patterns of paramagnetic effects (see accompanying paper). Nevertheless, it must be reiterated that no high-resolution structural data have, as yet, been obtained to confirm the structure of oxidized Pdx within a ~8-Å radius of the metal cluster. Delineation of the atomic resolution structure in this region must await either X-ray crystallographic analysis or replacement of the iron–sulfur cluster with a diamagnetic prosthetic group that does not introduce significant structural perturbations.

*Constraints Based on Paramagnetic Broadening Patterns.* Observed patterns of paramagnetic broadening were used to loosely constrain the position of the metal cluster with respect to the broadened resonances of five residues, Ser 22, Met 70, Leu 71, Val 74, and Gln 105. Paramagnetic broadening exhibits a $r^{-6}$ dependence on the distance between the paramagnetic site and the observed nucleus (Phillips & Poe, 1973). Oh and Markley (1990) noted that resonances closer than ca. 8 Å to the metal center in the *Anabaena* ferredoxin were not observable in two-dimensional spectra. The hyperfine-shifted resonances observed in the $^1H$ spectrum of oxidized Pdx are similar to those observed in the spectrum of oxidized *Anabaena* 7120 ferredoxin (Ratnaswamy & Pochapsky, 1993; Skjeldal et al., 1990). On the basis of this similarity as well as comparable patterns of hyperfine broadening in homologous structural features in the two proteins, 8 Å was taken as a rough limit for paramagnetic broadening in oxidized Pdx as well (Ratnaswamy & Pochapsky, 1993). The $C_\beta H_2$ resonances of Met 70 and the $C_\alpha H$ and $C_\beta H_2$ resonances of Leu 71, which were not observed in oxidized Pdx due to hyperfine interactions, were constrained to a distance no further than 8 Å from the nearest metal atom. As with NOE constraints, van der Waals radii were used as the close-approach limit and violations of 0.3 Å in excess were permitted without energy penalty.

Comparison of broadening patterns in the oxidized and reduced proteins suggests that the radius of the volume containing spins that are broadened beyond observability increases by ca. 1 Å (to about 9 Å) in reduced Pdx over that observed in the oxidized form (see accompanying paper). In particular, three resonances have been identified as being broadened more in the reduced than in the oxidized protein: the $C_\alpha H$ of Ser 22, the $C_\alpha H$ of Gln 105, and the $C_{\gamma 1}H_3$ of Val 74. In the reduced form, Ser 22 $C_\alpha H$ is significantly broadened and loses NOE connectivities and Gln 105 $C_\alpha H$ is also broadened but retains some weak NOESY and COSY connectivities, while the Val 74 methyl group resonance is completely lost. These three resonances were therefore constrained to be no closer than 8 Å but no further than 11 Å from the nearest iron atom in the oxidized protein.

*Structural Calculations.* Structural calculations were performed using the X-PLOR package (A. Brünger, Yale University) operating on a Silicon Graphics Iris Crimson workstation. A modification of the simulated annealing protocol of Nilges et al. (1988) was used. A structure consisting of the correct polypeptide sequence and appropriate connectivities for the $Fe_2S_2Cys_4$ cluster (ligation of iron atoms by the $S_\gamma$ atoms of Cys 39, Cys 45, Cys 48, and Cys 86) was generated with random $\phi$ and $\psi$ angles as a starting point. NOE constraints were represented as soft potentials, such that the energy increased linearly with deviation from allowed values. Dihedral angle constraints were set up as square-well potentials with a force constant of 1 kcal/mol rad$^2$. Energetic penalties were proportional to the square of the angular deviation.

Structures were heated to 1500 K after an initial minimization (5000 steps) for 60 000 steps of Verlet dynamics ($\Delta t$ = 3 fs) using experimental constraints but with reduced van der Waals repulsion terms. For the first 40 000 steps, required geometries were applied less stringently than during the last 20 000 steps. During the annealing phase (30 000 steps, $\Delta t$

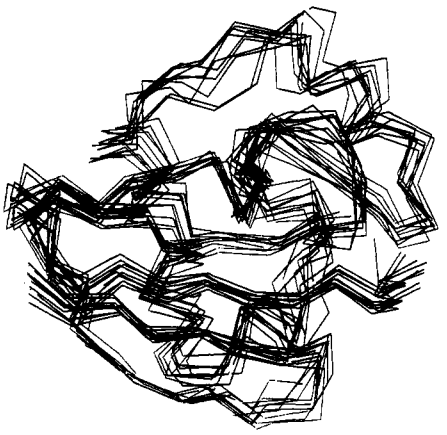

FIGURE 6: $\alpha$-Carbon connectivities for a family of 10 structures generated for oxidized Pdx. A pairwise rms deviation of 1.14 Å from the average atomic position was obtained for all backbone atoms and a 1.80-Å pairwise rms deviation from average structure obtained for all non-hydrogen atoms.

= 3 fs, $T_{final}$ = 100 K), van der Waals repulsive terms were gradually increased to their full values. A final minimization (10 000 steps) was then performed with all constraints and van der Waals terms active. Structures were examined after the first cycle in order to ensure the absence of gross errors (i.e., knots); if acceptable, the structures were further refined. Typically, two or three iterations of the protocol were sufficient to generate an acceptable structure, as determined by the absence of NOE violations greater than 0.5 Å or dihedral angle constraint violations greater than 5°.

The current level of structural refinement involved the use of generated structures to predict NOEs that, once identified in NOESY spectra, were added to the constraints list used for the dynamics calculations.

Ribbon figures were prepared using the MOLSCRIPT program (Kraulis, 1991).

## RESULTS

A family of 10 structures for oxidized Pdx was calculated as described above (Figure 6). Figure 7a,b is Ramachandran plots of $\phi$–$\psi$ backbone dihedral angles observed for non-glycine residues in the 10 structures in Figure 6 (not including the N- and C-terminal residues). Of the non-glycine residues, only the C-terminal residue, Trp 106, gives rise to positive $\phi$ angles in seven of the 10 accepted structures. This variability of the $\phi$ angle of Trp 106 is consistent with the conformational freedom observed for that residue by fluorescence-quenching measurements (Stayton & Sligar, 1991).

*Features of the Pdx Solution Structure Model.* The structure of oxidized Pdx is diagrammed in Figure 4. Two roughly symmetric helical regions [residues 23–31 ($\alpha$-helix D) and residues 57–73 (helices F and G)] are arranged on either side of the proximal central $\beta$-strand (residues 87–90, strand J) and the iron–sulfur cluster. Helix D ends at Gly 31, but compact structure continues for a short stretch (Ile 32–Ile 35). Helix D adjoins the metal cluster-binding site near Met 24. Although no resonance has been definitively assigned for Met 24, a NOE between the $C_\alpha H$ proton of Leu 23 and the $C_\beta H_3$ of Ala 26 confirms that residues 23 and 24 form part of helix D (spectral overlap prevents the observation of a $C_\alpha H$–NH $i,i$ + 3 NOE between these residues).

Helix F starts with Ala 57 and breaks at Pro 61; strong NH–NH connectivities are observed from Asn 53 to Val 60, but the characteristic $C_\alpha H$–NH $i,i$ + 3 NOEs observed in regular $\alpha$-helices could not be identified from Ala 55 and Phe

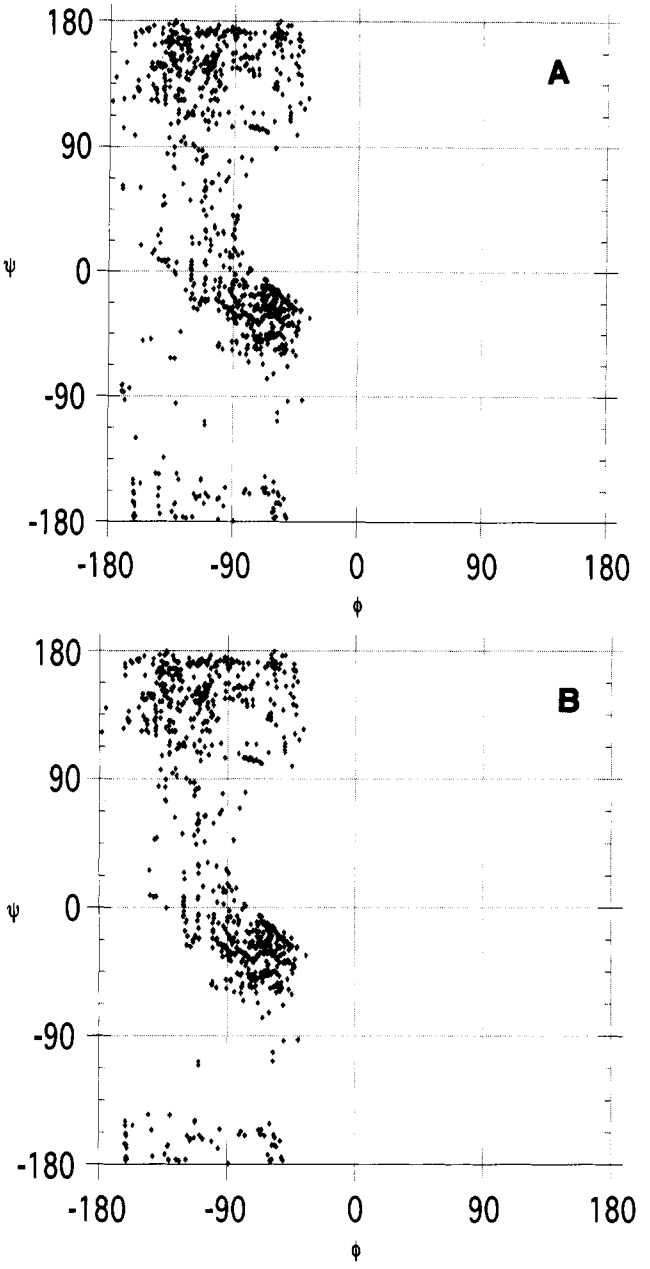


FIGURE 7: Ramachandran plots of $\phi$–$\psi$ angle sets for non-glycinyl residues in the family of 10 structures shown in Figure 6. Plot a shows $\phi$–$\psi$ angle sets for non-glycinyl residues from Lys 2 to Gln 105, including those in the vicinity of the metal cluster for which no NOE or coupling constraints are available. Plot B shows the same data except those residues in the metal cluster binding loop (Val 36–Cys 48) for which no NOE or coupling constraints are available.

56, although this may be due to spectral overlap. The $^3J_{NH-C_\alpha H}$ coupling constants for these two residues are also larger than expected for $\alpha$-helical residues (see Figure 3). A very weak NOE is observed from the $C_\alpha H$ of Ala 55 to the $C_\beta H$ of Asp 58, and a stronger NOE of the same type is observed between Phe 56 and Lys 59, so these residues apparently form a section of distorted helix. The side chain of Phe 56, the only phenylalanine in Pdx, forms part of the hydrophobic core of the protein. Asp 58, which has been implicated in the binding between Pdx and PdR, projects from helix F into solution (Geren et al., 1986). Three residues, Ala 62–Gln 64, provide a flexible loop that connects to helix G (Glu 65–Cys 73). Helix G contains residues Glu 65, Glu 67, and Glu 72, which have also been implicated in Pdx reductase binding (Geren et al., 1986) and the side chains of which are all solution exposed. The side chain of Cys 73 is partially solvent exposed,

which is unusual for a cysteine residue. Mass spectral data are consistent with considerable covalent modification of native Pdx with 2-hydroxyethanethiol (HET), presumably by formation of a disulfide bond (Kazanis et al., unpublished). HET is used as a preservative during purification and spectroscopy of Pdx. Such an observation is consistent with a surface-exposed cysteine. However, further work is required to confirm that Cys 73 is the site of such a modification.

Helix G adjoins the metal cluster near residues Met 70 and Leu 71 (as indicated by paramagnetic broadening of their resonances) and is connected to the type I turn H (Lys 79–Pro 80–Asn 81–Ser 82) by a short loop (Val 74–Leu 78). Turn H leads into one edge of an extensive $\beta$-sheet composed of five strands, A (Ser 1–Val 6), B (Arg 12–Val 17), L (Val 98–Val 101), E (Val 50–Asn 53), and I (Ser 82–Arg 83). One parallel (AL) and three antiparallel (AB, EL, and EI) strand arrangements are found in this sheet, which along with helix D show significant structural homology with the *Anabaena* 7120 ferredoxin (Figures 4 and 5). Much of the hydrophobic core of the protein is formed by the proximal (inward-facing) side chains of this sheet, including those of Val 3, Tyr 5, Leu 15, Val 50, Val 52, Ile 97, Val 99, and Val 101. Also integral to the core of the protein are the side chains of Leu 23, Ile 32, Phe 56, Thr 57, Met 90, and Leu 94. The Phe 56 ring packs close to strand L of the sheet, giving rise to large upfield chemical shifts for the $C_\alpha H$ of Ile 97 and the NH of Val 98 (Pochapsky & Ye, 1991). Similarly, interactions between the hydroxyphenyl ring of Tyr 5, the $\gamma_1$ methyl of Val 3, and the $\delta_1$ methyl of Ile 32 account for the significant upfield shifts observed for these methyl groups.

A second type I $\beta$-turn, K (Thr 91–Pro 92–Glu 93–Leu 94), connects the proximal central strand (residues 86–90) through a short stretch of irregular structure (residues 95 and 96) to the central strand L of the large $\beta$-sheet, which consists of residues 97–101 (vide supra). Residues Ile 89 and Met 90 of the proximal strand form a short stretch, J, of antiparallel $\beta$-sheet with Val 21 and Ser 22 (C).

A second compact region is formed by the side chains of His 49, Tyr 51, Val 74, Ala 76, Leu 78, and the C-terminal peptide Pro 102–Trp 106. The side chains of His 49 and Tyr 51, projecting from the distal face of the large $\beta$-sheet, contact the hydrophobic side chains of residues Val 74, Ala 76, and Leu 78 in the loop connecting helix G to turn H. The C-terminal loop (Pro 102–Trp 106) also contributes to the formation of this compact region. Slow exchange between bulk water and the hydroxyl proton of Ser 82, which is in proximity to the side chains of Tyr 51 and His 49, indicates limited access of solvent to this region. Very large downfield chemical shifts of both the Ser 82 OH proton and the His 49 $N_\delta H$ suggest some polarizing interaction that affects these resonances. The possibility of a secondary metal ion-binding site involving the side chains of His 49, Tyr 51, Ser 82, and possibly Lys 79 was considered, but elemental analysis of purified putidaredoxin did not indicate significant amounts of any common metal except iron. Another possibility is that a hydrogen-bonding network connects these residues, stabilizing the tertiary structure of this region of the protein.

The environment of the C-terminal residue, Trp 106, is of particular interest; it has been shown that Trp 106 is required for Pdx to retain full biological activity (Davies et al., 1990). In the accompanying paper, we describe the environment of the C-terminal region in some detail, noting NOEs between the $C_{\delta 1}H$ and $N_{\epsilon 2}H$ of the indole ring of Trp 106 with a side-chain methyl resonance of Val 74 and one unidentified methyl resonance, which the present structural model suggests could

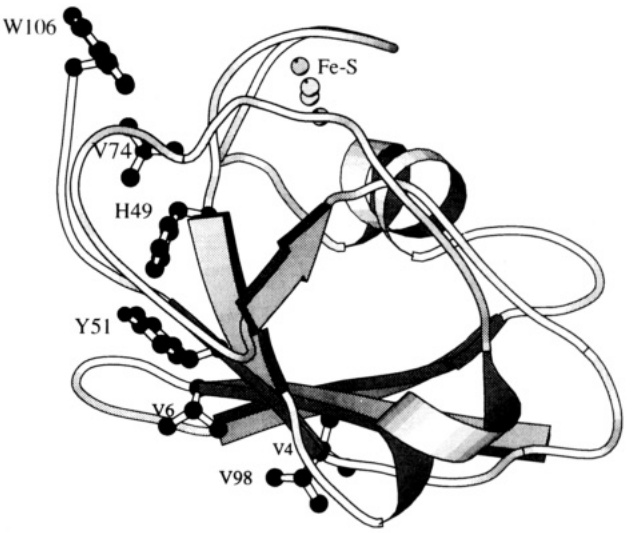


FIGURE 8: Features of Pdx structure proposed to be involved in binding interactions with cytochrome P-$450_{cam}$ (see text). Features include the side chains of Val 4, Val 6, Val 98, and Trp 106 and the partially buried side chains of Val 74, His 49, and Tyr 51.

be the $C_\beta H_3$ group of Ala 46. Recent experiments by Davies and Sligar indicate that the presence of an aromatic residue at the C-terminus is required for binding to P-$450_{cam}$ (Davies & Sligar, 1992). We have previously proposed that aromatic residues might be important mediators of protein–protein interactions, due to their high surface area (generating a significant hydrophobic driving force for binding) and the smaller loss of conformational entropy required to immobilize an aromatic residue relative to a less rigid side chain such as leucine or lysine (Pochapsky & Gopen, 1992). Fluorescence-quenching measurements indicate that, in free Pdx, the indole of Trp 106 is solvent exposed but becomes sequestered from solvent upon binding to P-$450_{cam}$ (Sligar et al., 1974b). It therefore seems reasonable to use the indole side chain of Trp 106 as a marker for the P-$450_{cam}$ binding site on Pdx. The solvent-exposed side chains of Val 4, Val 6, and Val 98 have also been proposed to be involved in the binding of P-$450_{cam}$ (Pochapsky & Ye, 1991). Figure 8 shows the structural relationships of these residues, indicating a possible Pdx/P-$450_{cam}$ binding interface.

A final observation in connection with the C-terminal tryptophan should be made; in neither oxidation state of Pdx has significant hyperfine broadening of the resonances of Trp 106 been observed, although the indole protons in the reduced form relax somewhat more rapidly than those in the oxidized protein (Pochapsky et al., accompanying paper). The structural model presented here places the $N_\epsilon H$ of Trp 106 between 8 and 10 Å from the nearest iron atom, which is consistent with a small increase in relaxation rate due to increased unpaired electron-spin density in the reduced protein. The absence of observable line broadening to this resonance suggests, however, that the $N_\epsilon H$ proton of Trp 106 spends only a fraction of the total time at this position. In any case, these observations argue against any mechanism for electron transfer that involves direct contact between the metal center and the C-terminal tryptophan unless a gross conformational change occurs upon binding (Baldwin et al., 1991; Halliwell, 1991).

*Limitations on the Model.* The most important limitation on this structural model is the absence of detailed data for the metal cluster and environment. We have attempted to make as few assumptions as possible in modeling the metal cluster; only those constraints that have been found to be strictly

necessary to satisfy the stereochemical and compactness requirements have been used. We note that most structures that were rejected for NOE constraint violations showed noncompact metal binding-site structures as well. Nevertheless, any conclusions based on specific features of the metal cluster-binding region are unwarranted. This region is shaded in Figure 4.

Paramagnetic effects also diminish the number of interdomain NOEs observed between resonances of protons on helix G and other regions of the protein. Much of helix G is in proximity to the metal-binding site, and the apparent mobility of that helix displayed in the various structural calculations may be to some extent an artifact of the lack of interdomain NOE constraints (vide infra).

Another limitation that the present model shares with any structure derived from NMR data is that the model is biased toward conformations that give rise to long-range NOEs. This is not a problem for regions of the protein such as the hydrophobic core, where equilibrium positions of atoms are apt to be well defined. However, for regions of the protein that exhibit conformational heterogeneity, only those conformers that give rise to long-range NOEs will be represented in the ensemble of structures; conformations that do not give rise to these NOEs will not be represented. This may be particularly important for the C-terminal region of Pdx, which has been shown to occupy more than one conformation by tryptophan fluorescence-decay measurements (Stayton & Sligar, 1991). Another region of the protein that may show structural heterogeneity is the loop containing His 8, Asp 9, Gly 10, and Thr 11. Inspection of the superimposed models in Figure 6 shows this region to adopt a number of conformations that satisfy the observed NOEs, which possibly reflect the time-average structure of this region rather than any one discrete conformer.

## CONCLUSIONS

The present results provide a basis for more detailed investigations of structure/activity relationships in the Pdx/P-450$_{cam}$ monooxygenase couple than were previously possible. They also represent the first structural characterization of an important class of ferredoxins which transfer electrons to monooxygenases. Other members of this class include adrenodoxin, terpredoxin, and linredoxin (Tanaka et al., 1973; Berg et al., 1976; Ullah et al., 1983). We are convinced that these results represent the most precise structural model for oxidized Pdx possible using only $^1$H NMR data. Coupling information obtained from the PE-COSY experiment is of limited usefulness in confirming stereochemistry and side-chain conformations because of spectral overlap; the best examples of this type of conformational analysis are obtained using much smaller proteins [e.g., Kraulis et al. (1989)]. Although only 90 of the 106 residues of Pdx contribute to the diamagnetic two-dimensional NOESY spectra, spectral overlap is sufficient to prevent identification of substantially more NOE constraints using the present methods. Further refinements in the structural model will require the use of multidimensional NMR methods with uniform and selective isotopic labeling to allow confirmation of stereospecific assignments, increase the number of dihedral angle constraints, decrease spectral overlap, and permit identification of further NOE constraints.

## ACKNOWLEDGMENT

The authors thank Thomas Branham for help in setting up the structural calculations, Hazel Holden for access to the *Anabaena* 7120 ferredoxin crystal structure, and Susan Sondej Pochapsky for performing the NOE buildup experiments. We also thank G. Petsko and D. Ringe for access to software, D. Peisach for help with graphics programs, and S. G. Sligar and J. T. LeComte for stimulating discussion.

## SUPPLEMENTARY MATERIAL AVAILABLE

List of NOEs used as constraints in structural calculations (11 pages). Ordering information is available on any current masthead page.

## REFERENCES

Arseniev, A., Schultze, P., Wörgötter, E., Braun, W., Wagner, G., Vašák, M., Kägi, J. H. R., & Wüthrich, K. (1988) *J. Mol. Biol. 201*, 637–657.

Baldwin, J. E., Morris, G. M., & Richards, W. G. (1991) *Proc. R. Soc. London, B 245*, 43–51.

Beratan, D. N., Onuchic, J. N., Winkler, J. R., & Gray, H. B. (1992) *Science 258*, 1740–1741.

Berg, A., Gustafsson, J.-Å., Ingelman-Sundberg, M., & Carlstrom, K. (1976) *J. Biol. Chem. 251*, 2831–2838.

Correll, C. C., Batie, C. J., Ballou, D. P., & Ludwig, M. L. (1992) *Science 258*, 1604–1610.

Cushman, D. W., Tsai, R. L., & Gunsalus, I. C. (1967) *Biochem. Biophys. Res. Commun. 26*, 577–583.

Davies, M. D., & Sligar, S. G. (1992) *Biochemistry 31*, 11383–11389.

Davies, M. D., Qin, L., Beck, J. L., Suslick, K. S., Koga, H., Horiuchi, T., & Sligar, S. G. (1990) *J. Am. Chem. Soc. 112*, 7396–7398.

Deisenhofer, J., Epp, O., Miki, K., Huber, R., & Michel, H. (1985) *Nature 318*, 618–624.

Dixon, D. W., & Hong, X. (1990) *Electron Transfer in Biology and in the Solid State, Advances in Chemistry 226*, p 164, American Chemical Society, Washington, DC.

Dixon, D. W., Hong, X., & Woehler, S. E. (1989) *Biophys. J. 56*, 339–351.

Dugad, L. B., La Mar, G. N., Banci, L., & Bertini, I. (1990) *Biochemistry 29*, 2263–2271.

Fu, W., Drozdzewski, P. M., Davies, M. D., Sligar, S. G., & Johnson, M. K. (1992) *J. Biol. Chem. 267*, 15502–15510.

Gerber, N. C., Horiuchi, T., Koga, H., & Sligar, S. G. (1990) *Biochem. Biophys. Res. Commun. 169*, 1016–1020.

Geren, L., Tuls, J., O'Brien, P., Millett, F., & Peterson, J. A. (1986) *J. Biol. Chem. 261*, 15491–15495.

Gunsalus, I. C., & Sligar, S. G. (1978) *Advances in Enzymology 47*, pp 1–44, Wiley Interscience, New York.

Halliwell, B. (1991) *Nature 354*, 191–192.

Kline, T. P., Brown, F. K., Brown, S. C., Jeffs, P. W., Kopple, K. D., & Mueller, L. (1990) *Biochemistry 29*, 7805–7813.

Koga, H., Yamaguchi, E., Matsunaga, K., Aramaki, H., & Horiuchi, T. (1989) *J. Biochem. (Tokyo) 106*, 831–836.

Kraulis, P. J. (1991) *J. Appl. Crystallogr. 24*, 946–950.

Kraulis, P. J., Clore, G. M., Nilges, M., Jones, T. A., Pettersson, G., Knowles, J., & Gronenborn, A. M. (1989) *Biochemistry 28*, 7241–7257.

Kumar, A., Ernst, R. R., & Wüthrich, K. (1980) *Biochem. Biophys. Res. Commun. 95*, 1–6.

Lipscomb, J. D., Sligar, S. G., Namvedt, M. J., & Gunsalus, I. C. (1976) *J. Biol. Chem. 251*, 1116–1124.

Ludvigsen, S., Andersen, K. V., & Poulsen, F. M. (1991) *J. Mol. Biol. 217*, 731–736.

Marion, D., & Bax, A. (1988) *J. Magn. Reson. 80*, 528–533.

Mayerle, J. J., Denmark, S. E., DePamphilis, B. V., Ibers, J. A., & Holm, R. H. (1975) *J. Am. Chem. Soc. 97*, 1032–1045.

McLendon, G. (1988) *Acc. Chem. Res. 21*, 160–167.

Moser, C. C., Keske, J. M., Warncke, K., Farid, R. S., & Dutton, P. L. (1992) *Nature 355*, 796–802.

Mueller, L. (1987) *J. Magn. Reson. 72*, 191–196.

Murray, R. I., Fisher, M. T., DeBrunner, P. G., & Sligar, S. G. (1985) *Top. Mol. Struct. Biol. 6*, 157–206.
Nagayama, K., & Wüthrich, K. (1981) *Eur. J. Biochem. 115*, 653–657.
Nilges, M., Clore, G. M., & Gronenborn, A. M. (1988) *FEBS Lett. 229*, 317–324.
Oh, B.-H., & Markley, J. L. (1990) *Biochemistry 29*, 3993–4004.
Pardi, A., Billeter, M., & Wüthrich, K. (1984) *J. Mol. Biol. 180*, 741–751.
Pelletier, H., & Kraut, J. (1992) *Science 258*, 1748–1755.
Phillips, W. D., & Poe, M. (1973) in *Iron Sulfur Proteins* (Lovenburg, W., Ed.) Vol. II, pp 255–284, Academic Press, New York.
Pochapsky, T. C., & Ye, X. M. (1991) *Biochemistry 30*, 3850–3856.
Pochapsky, T. C., & Gopen, Q. (1992) *Protein Sci. 1*, 786–795.
Pochapsky, T. C., Ratnaswamy, G., & Patera, A. (1994) *Biochemistry* (following article in this issue).
Poe, M., Phillips, W. D., Glickson, J. D., McDonald, C. C., & San Pietro, A. (1971) *Proc. Natl. Acad. Sci. U.S.A 68*, 68.
Poulos, T. L., Finzel, B. C., & Howard, A. J. (1987) *J. Mol. Biol. 195*, 687–700.
Rance, M., Chazin, W. J., Dalvit, C., & Wright, P. E. (1989) *Methods Enzymol. 176*, 114–134.
Ravichandran, K. G., Boddupalli, S. S., Hasemann, C. A., Peterson, J. A., & Deisenhofer, J. (1993) *Science 261*, 731–736.
Ratnaswamy, G., & Pochapsky, T. C. (1993) *Magn. Reson. Chem. 31*, S73–S77.
Ryckaert, J.-P., Ciccotti, G., & Berendsen, H. J. C. (1977) *J. Comput. Phys. 23*, 327–341.
Rypniewski, W. R., Breiter, D. R., Benning, M. W., Wesenberg, G., Oh, B.-H., Markley, J. L., Rayment, I., & Holden, H. M. (1991) *Biochemistry 30*, 4126–4131.
Skjeldal, L., Westler, W. M., & Markley, J. L. (1990) *Arch. Biochem. Biophys. 278*, 482–485.
Sligar, S. G., & Gunsalus, I. C. (1976) *Proc. Natl. Acad. Sci. U.S.A. 73*, 1078–1082.
Sligar, S. G., DeBrunner, P. G., Lipscomb, J. D., & Gunsalus, I. C. (1974a) *Int. Conf. Biochem. 9th*, Abstr. 7c12, p 339.
Sligar, S. G., DeBrunner, P. G., Lipscomb, J. D., Namtvedt, M. J., & Gunsalus, I. C. (1974b) *Proc. Natl. Acad. Sci. U.S.A. 71*, 3906–3910.
Smith, L. J., Sutcliffe, M. J., Redfield, C., & Dobson, C. M. (1991) *Biochemistry 30*, 986–996.
States, D. J., Haberkorn, R. A., & Ruben, D. J. (1982) *J. Magn. Reson. 48*, 286–292.
Stayton, P. S., & Sligar, S. G. (1990) *Biochemistry 29*, 7381–7386.
Stayton, P. S., & Sligar, S. G. (1991) *Biochemistry 30*, 1845–1851.
Tanaka, M., Haniu, M., Yasunobu, K. T., & Kimura, T. (1973) *J. Biol. Chem. 248*, 1141–1157.
Thomson, A. J. (1991) *Nature 350*, 22–23.
Tsukihara, T., Fukuyama, K., Nakamura, M., Katsube, Y., Tanaka, N., Kakudo, M., Wada, K., Hase, T., & Matsubara, H. (1981) *J. Biochem. 90*, 1763–1773.
Ullah, A. H. J., Bhattacharyya, P. K., Bakthavachalam, J., Wagner, G. C., & Gunsalus, I. C. (1983) *Fed. Proc. 42*, 1897.
Williams, R. J. P. (1990) *Electron Transfer in Biology and in the Solid State, Advances in Chemistry 226*, p 3, American Chemical Society, Washington, DC.
Wüthrich, K., Billeter, M., & Braun, W. (1983) *J. Mol. Biol. 169*, 949–961.
Ye, X. M., Pochapsky, T. C., Pochapsky, S. S. (1992) *Biochemistry 31*, 1961–1968.
Zuiderweg, E. R. P., Boelens, R., & Kaptein, R. (1985) *Biopolymers 24*, 601–611.